ORIGINAL RESEARCH

Radiosensitization with Gadolinium Chelate-Coated Gold Nanoparticles Prevents Aggressiveness and Invasiveness in Glioblastoma

Maxime Durand[1], Alicia Chateau[1,*], Justine Jubréaux[1,*], Jérôme Devy[2], Héna Paquot[1], Gautier Laurent[3], Rana Bazzi[3], Stéphane Roux[3], Nicolas Richet [iD][4], Aurélie Reinhard-Ruch[1], Pascal Chastagner[1,5], Sophie Pinel [iD][1]

[1]Université de Lorraine, CNRS, CRAN, Nancy, F-54000, France; [2]Université de Reims-Champagne-Ardenne, UMR CNRS/URCA 7369, MEDyC, Reims, F-51100, France; [3]Université Bourgogne Franche-Comté, UMR 6213 CNRS-UBFC, UTINAM, Besançon, F-25000, France; [4]Université de Reims-Champagne-Ardenne, Plateau Technique Mobile de Cytométrie Environnementale MOBICYTE Mobicyte, Reims, F-51100, France; [5]CHRU de Nancy, Hôpital d'enfants - Brabois, Vandoeuvre-lès-Nancy, F-54500, France

*These authors contributed equally to this work

Correspondence: Sophie Pinel, Email sophie.pinel@univ-lorraine.fr

Purpose: This study aimed to evaluate the radiosensitizing potential of Au@DTDTPA(Gd) nanoparticles when combined with conventional external X-ray irradiation (RT) to treat GBM.

Methods: Complementary biological models based on U87 spheroids including conventional 3D invasion assay, organotypic brain slice cultures, chronic cranial window model were implemented to investigate the impact of RT treatments (10 Gy single dose; 5×2 Gy or 2×5 Gy) combined with Au@DTDTPA(Gd) nanoparticles on tumor progression. The main tumor mass and its infiltrative area were analyzed. This work focused on the invading cancer cells after irradiation and their viability, aggressiveness, and recurrence potential were assessed using mitotic catastrophe quantification, MMP secretion analysis and neurosphere assays, respectively.

Results: In vitro clonogenic assays showed that Au@DTDTPA(Gd) nanoparticles exerted a radiosensitizing effect on U87 cells, and in vivo experiments suggested a benefit of the combined treatment "RT 2×5 Gy + Au@DTDTPA(Gd)" compared to RT alone. Invasion assays revealed that invasion distance tended to increase after irradiation alone, while the combined treatments were able to significantly reduce tumor invasion. Monitoring of U87-GFP tumor progression using organotypic cultures or intracerebral grafts confirmed the anti-invasive effect of Au@DTDTPA(Gd) on irradiated spheroids. Most importantly, the combination of Au@DTDTPA(Gd) with irradiation drastically reduced the number, the viability and the aggressiveness of tumor cells able to escape from U87 spheroids. Notably, the combined treatments significantly reduced the proportion of escaped cells with stem-like features that could cause recurrence.

Conclusion: Combining Au@DTDTPA(Gd) nanoparticles and X-ray radiotherapy appears as an attractive therapeutic strategy to decrease number, viability and aggressiveness of tumor cells that escape and can invade the surrounding brain parenchyma. Hence, Au@DTDTPA(Gd)-enhanced radiotherapy opens up interesting perspectives for glioblastoma treatment.

Keywords: gold nanoparticles, radiotherapy, brain tumor, cancer cell invasion, tumor recurrence

Introduction

Glioblastoma (GBM), the most common and aggressive brain malignancy in adults, is treated using a multimodal treatment including maximal safe surgical resection to the extent feasible, followed by radiation therapy with concomitant and adjuvant temozolomide-based chemotherapy. The major obstacle to a cure is diffuse invasion. Indeed, GBM is characterized by an invasive phenotype, which enables tumor cells to invade healthy brain areas and migrate along existing brain structures, including blood vessels, white matter tracts and meninges.[1] The highly migratory capabilities of these tumor cells are thought to be responsible for the short overall survival of GBM patients, since infiltrative cells escape treatments, notably from cytoreductive surgery, and may lead to recurrence. More worryingly, several papers have

Graphical Abstract
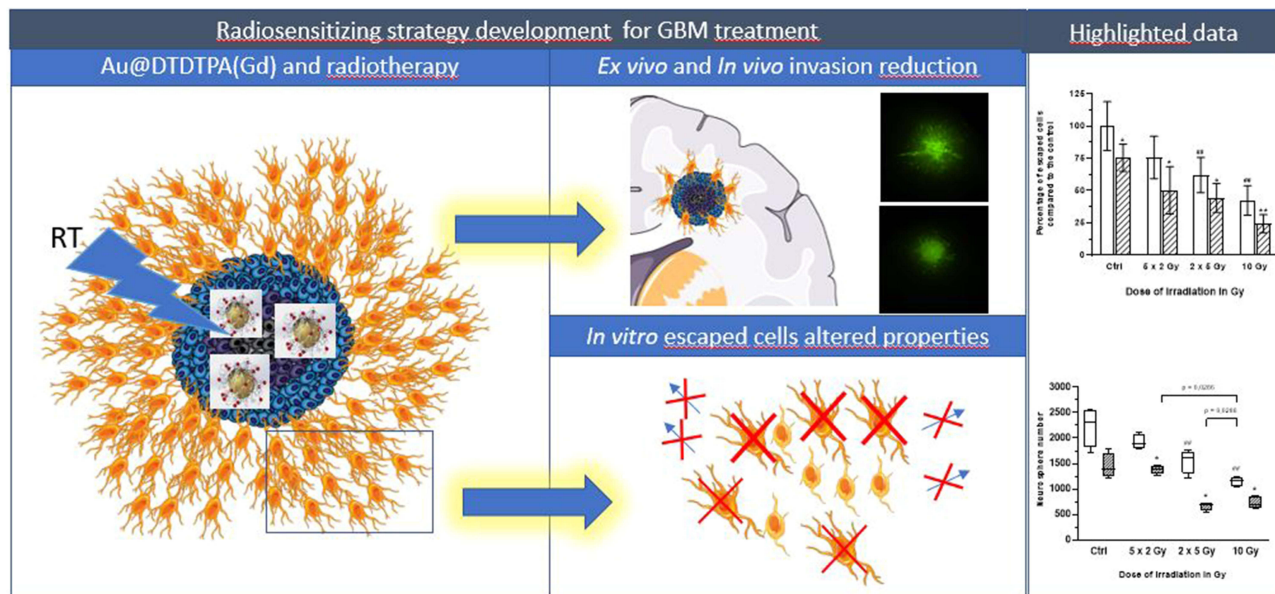
shown that conventional radiotherapy triggers a global adaptative response including increased migration/invasion ability of glioblastoma cells[2,3] with a phenotypic transition from proneural to the mesenchymal phenotype.[4]

Over the past decades, nanomedicine has brought forth many promising solutions for challenging glioblastoma management and has been expected to overcome their high treatment resistance.[5,6] Among the more recent innovations, many preclinical and clinical investigations are ongoing to evaluate metal-based nanoparticles as radioenhancer agents to treat radioresistant cancer including brain tumors.[7,8] Hafnium-based nanoparticles named as NBTXR3 have recently been approved in Europe as the first-in-class radioenhancer for the treatment of locally advanced soft tissue sarcoma (NBTXR3, Hensify®, Nanobiotix). Namely, high atomic element (Z) nanomaterials such as gold (Z = 79) and gadolinium (Z = 64) have gained widespread attention as dose enhancer in radiotherapy, due to their strong attenuation of photons, and their ability to increase the local deposition of radiation.[9–11] Although the radiosensitization effect of metal-based nanomaterials was initially attributed to this physical mechanism, an increasing number of studies challenge this mechanistic hypothesis and evidence the importance of chemical and biological contributions.[12,13]

In this context, Roux et al have developed the Au@DTDTPA(Gd) nanoparticles, which are ultrasmall polyamino-carboxylate-coated gold nanoparticles, then labelled with Gd^{3+} ions.[14] These nanoparticles exhibit a promising potential for MRI-guided radiotherapy.[15] Indeed, previous work has shown that (i) Au@DTDTPA(Gd) nanoparticles behaved as positive contrast agents for magnetic resonance imaging (MRI) and (ii) were able to improve the radioresponse of an intracranial 9L gliosarcoma model when the xenograft-bearing rats were treated with microbeam radiotherapy (MRT). MRT is a novel radiotherapy method based on a spatial fractionation of synchrotron-generated X-ray beams, allowing to deliver high-dose of irradiation at a very high rate with high-precision.

For further investigation, the present study aims at evaluating the radiosensitizing potential of Au@DTDTPA(Gd) nanoparticles when combined with more commonly used X-ray irradiation and closer to clinical treatments. Given the high invasiveness of glioblastoma, we have not only studied the effects of Au@DTDTPA(Gd) nanoparticles on the main tumor mass but also focused on the area of tumor extension. To answer this question, we have implemented complementary biological models (2D or 3D cell cultures, organotypic brain slice culture, orthotopic xenografts under chronic cranial windows…) and assessed the impact of combined treatments Au@DTDTPA(Gd) nanoparticles + RT on tumor progression considering various irradiation regimens. In an original way, we were interested in tumor cells with ability to

escape from the main tumor mass and infiltrate the healthy tissue in the context of irradiated tumors and showed how nanomedicine can help to minimize this process.

Materials and Methods
Cell Culture

The human primary glioblastoma cell line U87 (ATCC® HTB-14™, LGC Standard, France) was grown in Dulbecco's modified Eagle's Medium (DMEM) supplemented with 10% fetal bovine serum, 0.4% L-asparagine, 0.36% L-serine, 1% L-glutamine, 1% essential amino acids, 0.5% non-essential amino acids, 0.4% vitamins, 1.25% sodium pyruvate, and 1% penicillin–streptomycin. Cells were maintained in monolayers in a tissue culture incubator at 37°C under a 5% CO_2 95% air atmosphere and were subcultured twice a week. DMEM, amino acids, vitamins, and antibiotics were purchased from Gibco/Life Technologies (France), while other reagents were obtained from Sigma-Aldrich (Saint Quentin Fallavier, France). Cell counting was performed using a TC20™ automated cell counter (Bio-Rad, France) and viability assessment was determined using Trypan blue exclusion assay.

Au@DTDTPA(Gd) Nanoparticles

Au@DTDTPA(Gd) nanoparticles were synthesized and characterized as previously described in our published work.[16] For a typical preparation of gold nanoparticles, $HAuCl_4 \cdot 3H_2O$ (200 mg, 51×10^{-5} mol) was placed in a 250 mL round-bottom flask and was dissolved with methanol (60 mL). In another flask, DTDTPA (256 mg, 50×10^{-5} mol), water (40 mL) and acetic acid (2 mL) were mixed. This solution containing DTDTPA was added to the gold salt solution under stirring. The mixture turned from yellow to orange. $NaBH_4$ (195 mg, 515×10^{-5} mole) dissolved in water (13.2 mL) was added to the solution containing gold salt and DTDTPA under stirring at room temperature. At the beginning of the $NaBH_4$ addition, the solution first became dark brown then a black flocculate appeared. The vigorous stirring was maintained for 1h before adding aqueous hydrochloric acid solution (2 mL, 1 M). After the partial removal of the solvent under reduced pressure, the precipitate was retained on the polymer membrane and washed thoroughly and successively with 0.1 M hydrochloric acid, water and acetone. The resulting black powder was dried (up to 200 mg of dry powder of Au@DTDTPA) and dispersed in aqueous solution of sodium hydroxide (NaOH 0.01 M) to have a final concentration of 50 mM in gold.

The labeling by gadolinium ions is performed through the addition of $GdCl_3$ to colloidal solution under stirring at room temperature. For a final gold concentration of 45–50 mM, the gadolinium concentration is 5 mM.

Radiotherapy

Radiotherapy treatments were delivered using an X-Rad 320 (Precision X-Ray, USA) pre-clinical cabinet irradiator devoted to the irradiation of cell cultures and small animals in research. In vitro irradiation was performed using 160 kV energy X photon beams while in vivo irradiation used 320 kV energy X photon beams. The dose rate was 2 Gray (Gy)/ min. Various radiotherapy schedules were applied. For clonogenic assays, 2D cell cultures were irradiated at 2, 4, 6, or 10 Gy monodose. Irradiated spheroids received either a single dose of 2, 5 or 10 Gy at T8 or 5 fractions of 2 Gy (one fraction per day at T8, T9, T10, T11, T12) or 2 fractions of 5 Gy (at T8 and T11).

Clonogenic Assays

As previously described,[17] 1×10^5 U87 cells were plated in 25 cm² culture dish. Seventy-two hours after seeding, cells were incubated without or with Au@DTDTPA(Gd) nanoparticles (5 mM for 24h), washed twice with Hanks' Balanced Salt Solution (HBSS) and then irradiated at different doses (0, 2, 4, 6, 10 Gy) in fresh culture medium. A total of 10^4 cells were plated in soft-agar in 6-well plates and incubated for 12 days at 37°C under 5% CO_2. For improved contrast, surviving colonies were stained with 1 mL of MTT [3-(4,5-dimethylthiazol-2-yl)-2,5-diphenyltetrazolium bromide] solution (1 mg/ mL) and counted using GelCount™ device (Oxford Optronix, Abingdon, UK). Only colonies containing at least 50 cells were considered. Measurements were performed in triplicate, experiments were repeated five times. Results of clonogenic assays were plotted as survival curves showing the fraction of surviving cells as a function of the dose of ionizing radiation. The experimental data were fitted to a linear quadratic model, according to the equation $SF = e^{-(\alpha D + \beta D^2)}$ (with SF being the

Survival Fraction, D the dose of radiations in Gy and α, β radiobiological curve fitting factors, respectively). Dose modifying factor (DMF) was calculated for an isoeffect corresponding to SF = 75%.

Experimental Process for Obtaining Spheroids Culture and Escaped/Invading Cells

Supplementary Methods 1 summarizes the experimental process used to generate U87 or U87-GFP spheroids and escaped/invading cells. Briefly, 5×10^5 cells were plated in 75 cm^2 flasks previously coated with hydrophobic poly (2-hydroxyethyl methacrylate) (polyema) to prevent cell adhesion. Three days later, small cell clusters were harvested and placed in a spinner culture flask (T0) with magnetic stirring for 7 days to allow the spheroids to grow. On the seventh day (T7), the spheroid suspension was filtered through 380 and 520 µm nylon mesh filters in order to collect spheroids of homogeneous size (~400–500 µm).

After filtration, spheroids were seeded (i) in low-attachment 6-well plates to limit cell adhesion at a rate of 15 spheroids per well for most of experiments or (ii) in Labtek II™ 8 wells at a rate of 3 spheroids per well for immunocytochemistry. For the nanoparticles-treated groups, the spheroids were exposed to 5 mM Au@DTDTPA(Gd) nanoparticles for 24 hours. At T8, the culture medium containing Au@DTDTPA(Gd) nanoparticles was removed and, after gentle washing with HBSS, replaced with fresh culture medium. For the radiotherapy-receiving groups, the spheroids were treated on T8 or between T8 and T12 according to the irradiation schedule delivered (single dose vs fractionated irradiation). Meanwhile, under all conditions, many tumor cells escaped from the main tumor mass and adhered to the bottom of the flasks: we defined these as "escaped cells" or "invading cells". For most of experiments, the spheroids were harvested at T13, while the 'invading cells' were left in culture for a further 48 hours. At T15, the escaped cells were photographed using a transmitted light microscope (Nikon DIAPHOT 300 equipped with a Nikon Digital sight-DS-Fi1 camera; 40X magnification) before being harvested by trypsinization (trypsin with 0.05% EDTA ($^v/_v$)) for further assays.

Effect of Treatments on Spheroids' Size

After filtration, spheroids (~400–500 µm) were exposed to 5 mM Au@DTDTPA(Gd) nanoparticles for 24 hours. At T8, after gentle washing with HBSS, the spheroids received a 10 Gy monodose of X-ray radiation. Subsequently, the U87 spheroids were transferred and seeded individually into 96-well plates, previously coated with hydrophobic polyhema. On the day of seeding and 8 days later, each spheroid was imaged with the GelCount™ device allowing us to determine the volume of spheroids.

Conventional 3D Invasion Assays

Conventional 3D invasion assays have been carried out to determine the impact of radiotherapy on invasiveness properties of tumors, in presence or absence of Au@DTDTPA(Gd) nanoparticles. The influence of the X-photon dose and the influence of the fractionation regimen were assessed (Supplementary Methods 1). To evaluate the "dose effect", irradiated U87 spheroids received a single dose of 2 Gy, 5 Gy or 10 Gy at T8 and untreated or treated spheroids were harvested, just after treatment. To evaluate the "fractionation effect", we compared 3 schedules of irradiation at the total dose of 10 Gy: between T8 and T12, U87 spheroids were irradiated either at 10 Gy-monodose, with 2 fractions of 5 Gy (2 X 5 Gy) or with 5 fractions of 2 Gy (5 X 2 Gy) and untreated or treated U87 spheroids were recovered at T13. Conventional 3D invasion assays were performed and analysed as previously described,[16] (Supplementary Methods 2). Briefly, each spheroid was placed into individual well of 96-well plate and then embedded with 100 µL of a mix of Matrigel® and hyaluronic acid (100 µg/mL). Spheroids were maintained at 37°C in a humidified 5% CO2 atmosphere for 4 days, allowing invasion and migration processes to take place. For improved contrast, viable cells of the tumor core and invasion area were stained with MTT (1 mg/mL). Invasion was imaged using the GelCount® device (Oxford Optronix, UK) and quantified with ImageJ software: the total area of invasion (manual yellow delineation) and the core area (white delineation) as well as the invasion distance (µm) were determined.

Organotypic Brain Slice Cultures

The model of organotypic brain slice culture was adapted from the previously published protocols.[18] Six to eight-week-old nude mice were euthanized and the brains were isolated. After removing the cerebellum with a scalpel, each brain

was transferred to the vibratome (Leica VT1200 S) platform and immediately fixed to this device by applying a drop of superglue. The device was adjusted and the brain was placed facing the blade, in order to obtain 400 µm thick coronal slices with a maximal speed of 0.2 mm/s. At least 6 slices from each brain were collected and each one was positioned on interface-style Millicell® cell culture inserts (Merck Millipore, France) in 6 well culture plates containing 1 mL of sterile slice culture medium. The brain slice medium is composed of 50% DMEM, 25% HBSS, 25% heat-inactivated horse serum, 1 mM L- glutamine, 100 U/mL penicillin/streptomycin. Brain slices were incubated at 37°C under 5% CO_2 and the culture medium was changed from the bottom of each well every 2 days. Brain slices were prepared 48h before tumor implantation. At T8, the brain slices were breached with a 21G hypodermic needle and untreated or treated U87-GFP spheroids were deposited into the breaches using a pipet (defining the day of spheroid implantation Di). The organotypic brain slices cultures were maintained for at least 12 days.

Mitotic Catastrophe (MC) Detection

After harvesting, counting, and assessing the viability of escaped cells from U87 spheroids (at T15), cells were cytocentrifuged at a concentration of $2.5×10^4$ cells per slide for 1 minute at 500 rpm (Sakura, AutoSmear CF-12DE). The cells were then fixed in 10% neutral buffered formalin for 30 minutes. The slides were rinsed with PBS once. The slides were then stained with hematoxylin/eosin for visualization of nuclei. A mounting solution was deposited on the slides for histological staining preservation (Eukitt®). Snapshots of the slides were obtained at x10 magnification using an optical microscope (Nikon, DIAPHOT 300) equipped with a camera (Nikon, Digital sight-DS-Fi1). Ten pictures per slide were taken for data processing.

Imunocytofluorescence

At T15, escaped cells in Labtek™ II 8 wells were fixed with 4% ($^v/_v$) PFA for 30 minutes and then gently washed once with PBS. Cells were permeabilized with 0.1% ($^v/_v$) Triton-X-100 diluted in PBS for 10 minutes. The cells were gently rinsed for 5 minutes with PBS. Cells were saturated in 2% ($^w/_v$) bovine serum albumin (BSA) solution diluted in PBS for 1 hour. 150 µL of anti-connexin 43 primary antibody (rabbit polyclonal IgG, C6219, Sigma; dilution 1:400 in 2% PBS-BSA) was gently deposited into Labtek™ II wells. The antibody was incubated at 4°C overnight. The next day, slides were washed with PBS (3 times for 5 minutes). The Fc part of the primary antibody was detected with an Alexa Fluor 555-conjugated secondary antibody (Goat IgG anti-Rabbit IgG, Interchim, FP-SD5000; dilution 1:400 in 2% PBS-BSA). F-Actin was detected with Alexafluor-488-conjugated phalloidin (Ab176753, Abcam; dilution 1:1000 in 2% PBS-BSA). In practice, 150 µL of a mixed solution containing the Alexa Fluor 555-conjugated secondary antibody and the Alexafluor-488-conjugated phalloidin was deposited in Labtek II wells for 1 hour in the dark, at room temperature. The cells were then rinsed for 5 minutes with PBS, 3 times. Nuclei were counterstained with Hoechst 33432 (Thermo Scientific, 62249; dilution 1:1000 in PBS) for 15 minutes. Cells were rinsed once with PBS and then a solution against photobleaching (Ibidi, 50001) was applied before slide-lamellar mounting. Phalloidin and secondary antibody fluorescence were analyzed using an ImageXpress® Micro Confocal instrument with a 10x and 20x APO Plan objective and MetaXpress software (Molecular Devices, Sunnyvale, CA). Acquisitions were performed by exciting Alexafluor 488 and Alexafluor 555. The emitted fluorescence was detected in the appropriate wavelength window. Ten images were captured with a 0.2 µm z-step.

Zymography

For these experiments, after spheroid withdrawal at T13, culture medium of invading cells was replaced by reduced serum media (Opti-MEM I reduced serum medium, no phenol red, Gibco). Supernatants from the escaped cells were collected at T15 on ice and centrifuged at 300G for 10 minutes at 4°C to remove cell debris. The quantification of the secreted proteins in the supernatants was performed by colorimetric assay using Pierce™ BCA protein assay kit (Thermo Fisher Scientific, France). 4 µg of proteins were respectively deposited in a 10% polyacrylamide gel with 1% porcine gelatin (Sigma Aldrich, France). Proteins migrated for two hours at 4°C. Gelatinases were reactivated in a pH 7.6 buffer for 24 hours at 37°C. After staining with 0.2% Coomassie Blue (Thermo Fisher Scientific, France) for at least 15 min, MMP activity was revealed using a Doc XR+ Gel (Bio Rad, France). Densitometric quantification of the bands was performed with ImageJ software.

Neurosphere Assays

After recovery by trypsinization, escaped cells were seeded at a concentration of 1×10^5 cells per well in low-attachment 6-well plates. For neurosphere assays, the serum-free culture medium used was a DMEM-F12 medium containing 0.001% insulin ($^v/_v$), 1% penicillin/Streptomycin ($^v/_v$), 2% B27 reagent ($^v/_v$), 1% N2 reagent ($^v/_v$), 0.002% EGF ($^v/_v$), and 0.002% β FGF ($^v/_v$). Plates were placed at 37°C under a humid atmosphere diffusing 5% CO_2 for 4 days. At the end of experiments, for improved contrast, the formed floating neurospheres were stained by addition of 1 mL of MTT at a concentration of 1 mg/mL and incubated for 3 hours before revelation with the GelCount™ device (Oxford, Optronix). GelCount™software was used to count neurosphere and measure neurosphere size.

Analysis of Gene Expression by RT-qPCR

RNA extraction and cDNA synthesis were performed as described in Supplementary Methods 3. Among the 5 reference genes selected, GAPDH and RPL32 were identified as the most stable genes according RefFinder web-tool. The list of reference and targeted genes is given in Supplementary Methods 3. Quantitative reverse-transcription polymerase chain reaction (qRT-PCR) was performed with qPCRBIO SyGreen Blue Mix according to manufacturer instructions (PCRBIOSYSTEMS), in a Biorad CFX96 Touch thermocycler using the Bio-Rad CFX Maestro 2.3 software. Relative gene expression was calculated using the 2(-Delta Delta C(T)) Method.[19]

In vivo Experiments

The in vivo experiments were performed in the institution EU 0393 CRAN UMR 7039 (approval number D54-547-03). The experiments were performed on 6-week-old female homozygous *BALB/cAnNRj-Foxn1nu* nude mice (20–25 g in weight) (Janvier Lab, France). After evaluation by the "Comité d'Ethique Lorrain en Matière d'Expérimentation Animale" (CELMEA, C2EA-66) under the supervision of the *Ministère de l'Enseignement Supérieur et de la Recherche*, these experimental protocols have received the necessary ministerial authorizations (APAFIS numbers: 4776–2016040118263024. v4 and 14597–2018040722467360.v7) certifying that the housing conditions, the experiments and the surgical techniques implemented were in accordance with the ethics and legislation in force. All experiments (surgery, intravital microscopy observation, radiotherapy treatment) were performed on anaesthetized animals. Anaesthesia consisted of an intraperitoneal injection (5 μL/g body weight) of a mixture of ketamine (90 mg/kg, Imalgen 500, Merial, France) and xylazine (8 mg/kg, Rompun 2%, Bayer Health Care, France) diluted in water for injection.

Chronic Cranial Window Model

The chronic cranial window model (Supplementary Methods 4) is a model adapted from the previously published protocols that allows for longitudinal following of intracerebral tumor progression.[20–22] After anaesthesia, the mice were placed on a heating blanket and secured in a stereotaxic frame. A sterile ointment is applied to the eyes to prevent keratitis and the surgical site was cleaned by 0.2% chlorhexidine solution. A subcutaneous injection of 50 μL of 2% xylocaine was performed at the surgical site. To prevent the formation of cerebral oedema after surgery, an intramuscular administration of dexamethasone (20 μL of a 2 mg/mL solution) was performed in the quadriceps. An incision (half circle of about 1 cm^2) was carefully made over the skin of the right hemisphere and a skin flap as well as the periosteum were gently removed. Using a microdrill (Foredom®, MH 150, Phymep, France), a craniotomy corresponding to a circle of approximately 4 mm in diameter between the bregma, sagittal and lambdoid sutures was performed through careful drilling. The dura mater was quickly removed with fine forceps. In the center of the trepanning area, a breach was created within the cortex near a vascular network. A U87-GFP spheroid, approximately 450 μm in diameter, was deposited into the breach. For in vivo evaluation of treatment efficacy, we grafted U87-GFP spheroids immediately after filtration (ie, T7 of the spheroid process) whereas to study U87 tumor invasion after treatments, U87-GFP spheroids were treated in vitro prior to in vivo implantation (ie, T8 of the spheroid process) (Supplementary Methods 5).

To sterilely seal the trepanning hole, the brain was covered with a sterile circular glass slide (diameter 5 mm) fixed with cyanoacrylate glue (Histoacryl®, Braun, Spain) and dental acrylic (Mega dur, Megadental, GmbH, Germany). The cyanoacrylate glue, applied to the peripheral skull and the edges of the flap, was used to seal the bone flap. A thin layer of

dental acrylic was applied under the skin at the wound margins and also covering a small edge of the flap to strengthen fixation.

Intravital Microscopy

A Nikon AZ100 fluorescence microscope (Nikon, France) was used for longitudinal monitoring spheroid viability, growth and progression. Acquisition of fluorescence signals was performed in the appropriate wavelength window: for GFP (Exc 395 nm/Em 504 nm) and Cy5 (Exc 650 nm/Em 670 nm). Three or five days after surgery, a first imaging was performed to check the good vascularization of the spheroids, a prerequisite for their long-term viability. Intravital microscopy observations were repeated once a week.

In vivo Evaluation of Treatment Efficacy

Supplementary Methods 6 summarizes the experimental schedule used. Five days after spheroid implantation (Di), mice with well-vascularized tumor were randomly assigned to the different treatment groups and treatment was started, defining the D0 of the following. Au@DTDTPA(Gd) nanoparticles were injected intravenously at a dose of 75 mg/kg from a 10 g/L solution. Radiotherapy-treated mice received a 2×5 Gy schedule (ie, 5 Gy irradiation on D0 and D3). For the combined treatments, Au@DTDTPA(Gd) nanoparticles were administered 10 min before the first irradiation fraction. Tumor volumes (V) were calculated from the recorded fluorescence images, according to the equation $V = \frac{d^2 \times D}{2}$ where d and D represent the smallest and the largest diameter, respectively. Relative tumor volume (RTV) that helps to assess tumor growth rate, was determined by dividing tumor volume on day X by tumor volume on D0 (eg, RTV at day 30 = V_{D30}/V_{D0}).

Statistical Analysis

The Mann–Whitney *U*-test was used to compare untreated and treated groups. A *P*-value less than 0.05 was considered as statistically significant. #: represents statistically significant difference between the RT groups versus Ctrl group. *: represents statistically significant difference between Au@DTDTPA(Gd) group versus Ctrl group or between groups receiving combined treatment versus groups receiving irradiation alone.

Results

Radiosensitizing Potential of Au@DTDTPA(Gd) Nanoparticles

To assess the radiosensitizing effects of Au@DTDTPA(Gd) nanoparticles when combined with photon irradiation, a stepwise experimental approach from in vitro assays to in vivo studies was carried out to better investigate the intrinsic properties of cancer cells alone and within their microenvironment.

Thus, in a first time, the radiosensitizing potential of Au@DTDTPA(Gd) nanoparticles was evaluated in vitro by clonogenic assays on U87 glioblastoma cells. Figure 1A shows the radiation dose–response curves for U87 cells monolayers exposed or not to 5 mM of NPs for 24h: the proportion of surviving U87 cells irradiated at 2 Gy and 10 Gy was lower after exposure to gold nanoparticles (85% and 45%, respectively) than in the absence of gold nanoparticles (94% and 63%, respectively), and the dose modifying factor (DMF) reached 0.5.

In parallel, we studied the effects of the combined treatment (RT 10 Gy monodose + Au@DTDTPA(Gd) 5 mM for 24h) nanoparticles on 3D cell culture models and compared to the control group (no RT, no nanoparticles), the nanoparticles-receiving group and the RT-treated group (Figure 1B). The growth of U87 spheroids was monitored by optical microscopy for 1 week after treatments: it was shown that the volume of spheroids exposed to RT 10 Gy alone or to combined treatment RT+NPs was significantly reduced, as compared to untreated spheroids. Moreover, the spheroids receiving the combined treatment were significantly smaller than those treated by RT alone, signifying that Au@DTDTPA(Gd) nanoparticles were able to enhance the antitumor effect of X-ray irradiation.

These promising in vitro results led to in vivo experiments: for this purpose, we used an intracerebral xenograft model of U87-GFP spheroids under chronic cranial windows and a fractionated X-ray irradiation regimen (ie, RT 2×5 Gy). As the radiosensitizing effect depends mainly on the accumulation of nanoparticles in the tumor tissue, we first verified by intravital microscopy the presence of Cy5-labelled Au@DTDTPA(Gd) nanoparticles[23] in the intracerebral tumour after i.v. injection (Supplementary Figure 1).
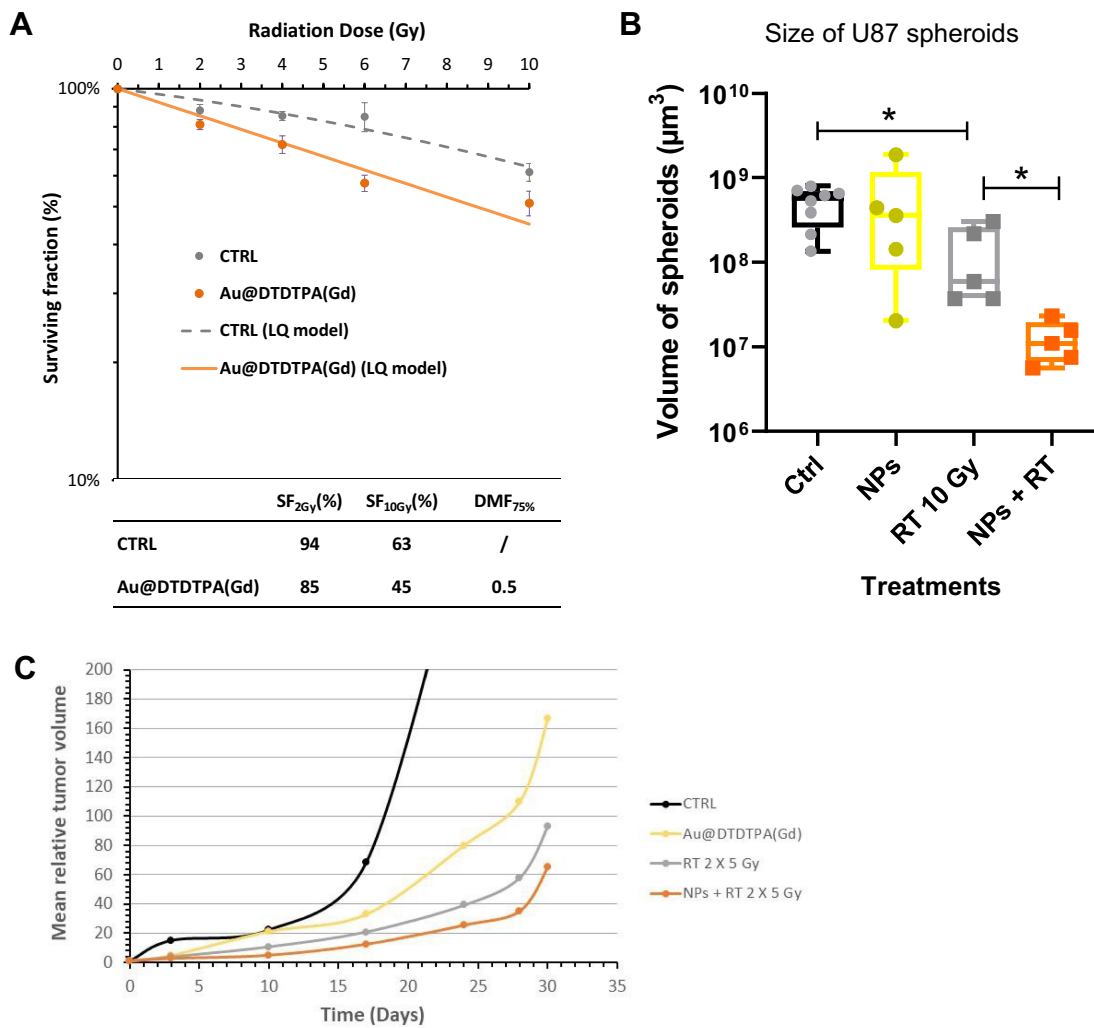
Figure 1 Radiosensitizing potential of Au@DTDTPA(Gd) nanoparticles. (**A**) Radiosensitizing effect assessed in vitro by clonogenic assays. U87 cells were incubated with 5 mM Au@DTDTPA(Gd) nanoparticles for 24 hours, washed twice with HBSS and then irradiated at different doses (0, 2, 4, 6, 10 Gy) in fresh culture medium. A total of 10^4 cells were plated in soft-agar in 6-well plates and incubated for 12 days at 37°C 5% CO_2. Surviving colonies containing at least 50 cells were counted using GelCount™ (Oxford Optronix, Abingdon, UK). Results of clonogenic assays were plotted as survival curves. The experimental data were fitted to a linear quadratic (LQ) model, according to the equation $SF = e^{-(\alpha D + \beta D^2)}$. SF_{2Gy} and SF_{10Gy} are respectively the surviving fractions at 2 and 10 Gy, respectively; DMF is the dose modifying factor. (**B**) Antitumor activity of treatments assessed in vitro using 3D cell culture models. After 7 days growth in spinner, U87 spheroids were seeded in low-attachment 6-well plates. They were exposed to 5 mM Au@DTDTPA(Gd) nanoparticles (NPs) for 24 hours at T7 and/or irradiated with 10 Gy-monodose (RT 10 Gy) on T8. Subsequently, the U87 spheroids were seeded individually into a precoated 96-well plates. Each spheroid was imaged and their volume determined on the day of seeding and 8 days later. Results are presented as boxplot of data (n ≥ 5). * = significant difference at p < 0.05 according to the Mann–Whitney *U*-test (**C**) In vivo evaluation of the effects of treatments on tumor progression. For in vivo experiments, we used an intracerebral xenograft model of U87-GFP spheroids under chronic cranial windows. Treatments started 5 days after spheroid implantation, thus defining the D0 of follow-up. The nanoparticles were injected intravenously at a dose of 75 mg/kg from a 10 g/L solution. Radiotherapy-treated mice received a 2×5 Gy regimen. For combined treatments, Au@DTDTPA(Gd) nanoparticles were administered 5 min before the first fraction of radiation. Intravital microscopy using a Nikon AZ100 fluorescence microscope (Nikon, France) allowed us to follow the progression of intracranial U87-GFP tumors. Based on the recorded fluorescence images, tumor volumes were determined and relative tumor volumes (RTV = V_{Dx}/V_{D0}) were calculated. The graph represents the mean tumor growth curve plotted for each treatment group.

Intravital microscopy through the chronic cranial window allowed for long-term monitoring of tumor growth and spread of U87 spheroids. Relative tumor volume (RTV) was determined based on the acquisition of fluorescence images and mean growth curve for each therapeutic group is plotted in Figure 1C. Regardless of the treatment group, U87-GFP tumors grew steadily to ethical endpoints within 40 days. Unfortunately, no local tumor control was obviously noticed but all treatments have slowed down tumor growth, as compared to the exponential growth of untreated-tumors. Combined treatment seemed slightly more efficient to delay tumor growth than radiotherapy alone. Indeed, mean RTV at D30 have reached 166.8 for NPs-treated tumors, 92.9 for RT-receiving mice and only 65.1 for tumors treated by RT+NPs. Consistently, the median time for tumors to reach RTV equal to 30 was 18.4 days for RT group vs 25.1 days for RT+NPs group (Table 1). In addition, on D20, 5

Table 1 Effects of Treatments on the Growth of U87 Intracerebral Tumor

Therapeutic Groups	Number of Days to Reach RTV = 30		RTV ≥ 30 Reached on D20	
	Median (in Days)	Range	Number of Animals	(Percentage)
Control	12.9	[4.5–23.5]	6/7	(85.7%)
Au@DTDTPA(Gd) NPs	18.6	[8–35.5]	6/8	(75.0%)
RT	18.4	[14.5–34.5]	5/8	(62.5%)
RT + NPs	25.3	[21.5–35]	0/8	(0.0%)

Notes: NPs: Mice received intraveneous injection of Au@DTDTPA(Gd) nanoparticles at a dose of 75 mg/kg. RT: 2 fractions of X-rays irradiation at 5 Gy on D0 and D3. RT + NPs: intraveneous injection of Au@DTDTPA(Gd) at 75 mg/kg 5 minutes before the first fraction of irradiation; 2 fractions of 5 Gy on D0 and D3. Based on the determination of tumor volume by intravital microscopy, two criteria were considered: the time (in days) taken for the relative tumor volume (RTV) to reach 30 and the number of mice whose RTV exceeded 30 on day 20 of follow-up.

out of 8 RT-treated mice exhibited RTV ≥30 while 0 out of 8 mice receiving combined treatment. Nevertheless, difference between RT and RT+NPs groups was not statistically significant, maybe because of the very heterogenous behavior of RT-treated tumors. Specifically, we noticed that the contouring of tumors and the volume determination appeared more difficult in RT-receiving mice, as the areas of tumor extension are less bright and more blurred than in other groups (Supplementary Figure 2). All these observations led us to pay more attention to the peripheral regions of the tumor and to evaluate the impact of treatments on the invasion process.

Anti-Invasive Effects of Au@DTDTPA(Gd) on Irradiated Cells

To address the invasion, invasion properties of U87 cells after treatments were examined using 3 distinct and complementary spheroid models: in the first one, untreated or treated U87 spheroids were embedded in a matrix composed of Matrigel® and hyaluronic acid, consistently with conventional "3D invasion assays"; the second model corresponded to organotypic brain slice cultures, allowing untreated or treated U87-GFP spheroids to grow in vitro into cerebral environment; and for the third model we have implanted a U87-GFP spheroid post in vitro treatment into brain parenchyma of mice under a cranial window for intravital microscopy-based monitoring.

Conventional 3D invasion assays were carried out to determine the impact of radiotherapy on the invasiveness of tumors, in presence or absence of Au@DTDTPA(Gd) nanoparticles. The influence of the X-photon dose (2 Gy, 5 Gy or 10 Gy) (Figure 2A) and the influence of the fractionation regimen (10 Gy-monodose, versus 2 fractions of 5 Gy (2 X 5 Gy) versus 5 fractions of 2 Gy (5 X 2 Gy)) were assessed (Figure 2B). The surface of tumor cores was slightly impacted by irradiation whatever the dose and the regimen considered, as compared to control group. Unexpectedly, radiotherapy failed to reduce tumor cell invasion in term of area or distance of invasion. In contrast, applying irradiation tended to increase the average surface or distance of invasion and the difference became statistically significant in particular for the 5×2 Gy regimen (793 ± 126 μm vs CTRL 525 ± 144 μm; p < 0.0001), which represents the usual clinical fractionation. Mean surfaces or distances of invasion were lower in RT+NP groups than in RT groups, suggesting that the combined treatments were efficient to interfere with glioblastoma cell invasiveness after irradiation. For example, the invasion area was only 1.67 ± 0.64 mm² when spheroids were treated by Au@DTDTPA(Gd) + 2×5 Gy irradiation while it reached 2.42 ± 0.67 mm² for 2×5 Gy irradiation alone (p = 0.003).

As this conventional in vitro model has limited the duration of monitoring, we attempted to confirm these results by alternative approaches. When untreated- or 10 Gy-irradiated U87-GFP spheroids were grafted onto organotypic brain slices, the progression of fluorescent tumor cells in cerebral environment was followed over 12 days after implantation (Figure 2C), allowing to visualize the growth of the central cores along with their infiltrating extensions. The sole exposition of spheroids to Au@DTDTPA(Gd) nanoparticles did not cause any change compared to control group; 10 Gy-irradiation induced the reduction of tumor growth with noticeable diffuse infiltration. By contrast, pre-treatment by Au@DTDTPA(Gd) of 10 Gy-irradiated spheroids resulted in diminished infiltrating area.
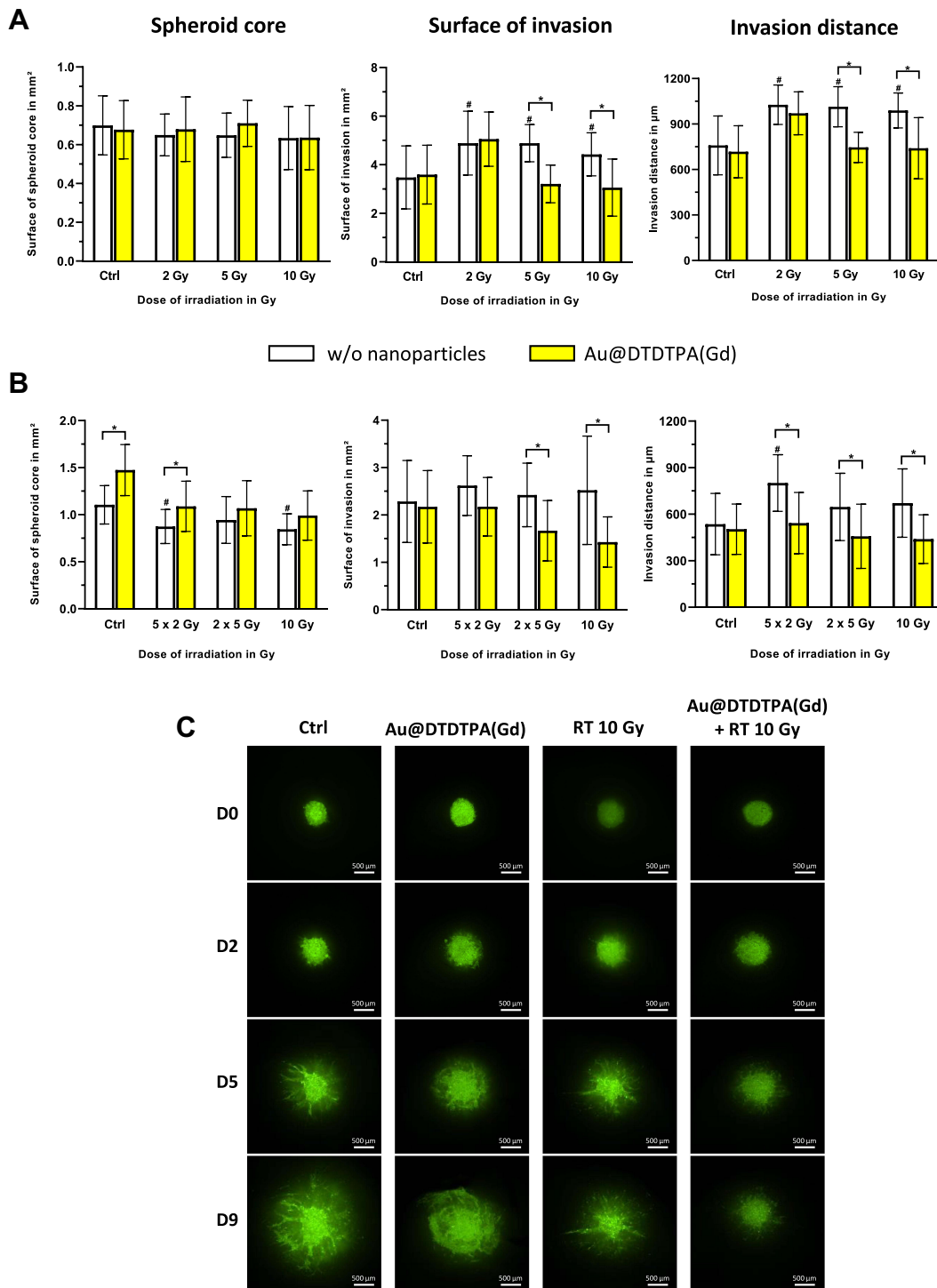
Figure 2 In vitro anti-invasive effects of Au@DTDTPA(Gd) on irradiated cells. After seeding in 6-well plates (15 spheroids per well), U87 spheroids were exposed 5 mM Au@DTDTPA(Gd) for 24 h and/or treated by X-photon irradiation (w/o = without nanoparticles). (**A**) Influence of the dose of radiation. Single-dose of radiotherapy (2, 5 or 10 Gy) was delivered on T8 and each spheroid was then placed into individual well of 96-well plate and then embedded with 100 μL of a mix of Matrigel® and hyaluronic acid (100 μg/mL). (**B**) Influence of the radiation fractionation. Irradiated spheroids received either 10 Gy-monodose, 2 fractions of 5 Gy (2 X 5 Gy) or 5 fractions of 2 Gy (5 X 2 Gy) between T8 and T12 and spheroids were embedded in matrix at T13. Four days later, invasion of viable cells was imaged using the GelCount® system (Oxford Optronix, UK). Histograms represent for each treatment condition the measurements of the surface of spheroid core (mm²), the invasion surface (mm²) and the invasion distance (μm). They were measured with ImageJ software. Results are presented as mean ± SD (n ≥ 12 spheroids for at least n ≥ 3 independent experiments). # = significant difference between RT groups versus Ctrl group and * = significant difference between "with Au@DTDTPA(Gd) nanoparticles" groups versus "w/o nanoparticles" groups at p < 0.05 according to the Mann–Whitney *U*-test. (**C**) Invasion after treatments have also been addressed using organotypic brain slice cultures, that allowed untreated or treated U87-GFP spheroids to grow in vitro into cerebral environment. Representative images acquired at Day 0 (D0), Day 2 (D2), Day 5 (D5), Day 9 (D9) using a Nikon AZ100 fluorescence microscope (Nikon, France) show the growth of the tumor core and the progression of invasive area. The scale bar is 500 μm (n ≥ 3 independent experiments).

To complete this, implantation of U87-GFP into the brain parenchyma under a cranial window allowed a longer-term follow-up (Supplementary Figure 3). Untreated spheroids and NPs-treated spheroids resulted in rapid growth of tumor mass, forcing the sacrifice of mice before day 30 of follow-up. In contrast, the in vivo environment revealed specific tumor behavior after radiation therapy. Ten Gy-irradiation induced a dramatic shrink of tumor mass until it almost disappeared; however, isolated tumor cells which escaped from the tumor bulk continued progressively disseminating into the brain parenchyma, causing disease symptoms (considered as ethical endpoints) after 75 days. When spheroids were treated by 10 Gy-irradiation plus Au@DTDTPA(Gd) nanoparticles, the glioblastoma cells disappeared, allowing the animals to remain alive until the end of the study (>4 months). Taken together, our results confirmed the anti-invasive effects of Au@DTDTPA(Gd) nanoparticles and demonstrated that nanoparticles could prevent tumor cells from escaping from the main tumor mass and disseminating into normal brain parenchyma.

Au@DTDTPA(Gd) Nanoparticles Reduced the Number of Invading Tumor Cells After Irradiation

Next, in vitro experiments were conducted to focus on invading cells that escape from U87 spheroids. Cell count at T15 revealed that fifteen U87 spheroids give rise to $1.59 \pm 0.27 \times 10^5$ invading tumor cells among which $80.2 \pm 4.4\%$ are viable cells (Figure 3A and B). These invading cells mainly formed new clusters all over the culture well (red arrows), and clusters were sometimes connected by membrane extensions emitted by isolated cells (Figure 3C).

For the irradiated spheroids, in addition to their slower growth, the number of invasive cells was significantly reduced as compared to control group, although the rate of inhibition depended on the treatment regimen. As expected, the single-dose schedule was the most effective in limiting tumor cell invasiveness. Indeed, the 10 Gy monodose treatment divided the number of invasive cells by a factor of 2.3 ($0.67 \pm 0.17 \times 10^5$ cells; p = 0.002) (Figure 3A) and induced a significant decrease of viability ($53.5 \pm 13.3\%$; p = 0.002) of the invading tumor cells (Figure 3B). The fractionated schedules (5 X 2 Gy and 2×5 Gy) reduced the number of invasive cells by approximately 25% and 40%, respectively. As the efficacy of radiation therapy increased, cell morphology became more altered: we observed many larger and more spread out cells and fewer tumor cell clusters (Figure 3C and Supplementary Figure 4A). It is noteworthy that escaped cells, although less numerous, remained connected through thin and ultralong membrane protrusions (ie, some exceeding 500 μm in length).

Fifteen U87 spheroids exposed to 5 mM of Au@DTDTPA(Gd) nanoparticles gave rise to $1.20 \pm 0.15 \times 10^5$ invading tumor cells, ie, 25% less than untreated spheroids (Figure 3A). The viability of invading cells was slightly affected by nanoparticles treatment ($73.7 \pm 5.6\%$; not statistically significant) (Figure 3B). In this condition, fewer clusters were detectable in the culture wells and isolated cells remained connected by membrane protrusions (Supplementary Figure 4A). Whatever the RT regimen considered, the association of nanoparticles with irradiation brought a significant benefit. Thus, the regimen 10 Gy monodose + NPs divided the number of invasive cells by a factor of 4.1, with only $0.39 \pm 0.10 \times 10^5$ cells escaped from 15 spheroids (Figure 3A) and the viability was less than 50% (Figure 3B). In this case, invading cell morphology was critically altered, no tumor cell clusters have been formed, and few smaller membrane extensions failed to connect remaining tumor cells together (Supplementary Figure 4A).

The low cell viability along with the altered morphology of invading cells have drawn our attention. So, we have carried out hematoxylin and eosin staining to characterize morphological alterations, focusing on abnormal cell nuclei, namely micro- and multinucleation, which are representative of mitotic catastrophe (Supplementary Figure 4B). The rate of MC for each therapeutic condition is presented in Figure 3D. While MC concerned only $7.5 \pm 0.7\%$ of escaped cells in control group, the rate of MC significantly increased after radiotherapy, whatever the irradiation schedule applied. Fractionated schedules led into $23.7 \pm 1.6\%$ (for 5×2 Gy) and $31.9 \pm 1.9\%$ of MC (for 2×5 Gy) and as expected, 10 Gy single-dose irradiation was the most effective regimen, inducing $37.5 \pm 2.5\%$ of MC. Exposure of spheroids to Au@DTDTPA(Gd) nanoparticles doubled the rate of MC in invasive cells ($14.8 \pm 1.4\%$, p = 0.008) as compared to control group and significantly enhanced MC events in case of fractionated irradiation (eg, $38.2 \pm 1.9\%$ for NPs + RT 2×5 Gy ; p = 0.007 compared to RT 2×5 Gy alone). Therefore, the decrease in viability of escaped cells was probably due to the increase in mitotic catastrophe after the treatments.
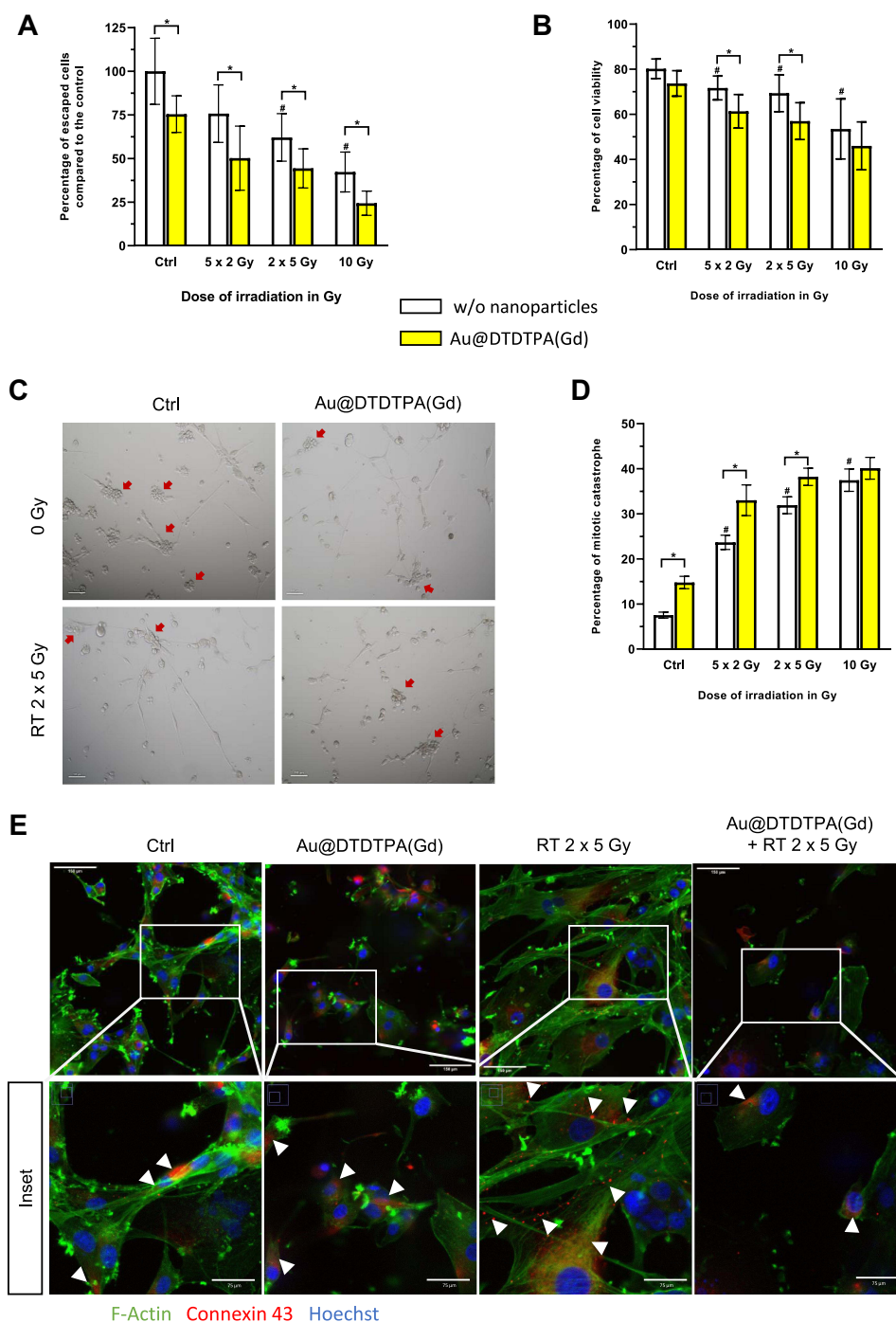
Figure 3 Impact of treatments on escaped tumor cells. Fifteen U87 spheroids were seeded per well. Many of tumor cells escaped from the spheroids and adhered to the bottom of the flasks: we defined them as "escaped cells" or "invading cells". (**A**) After trypsinization, recovered cells were counted and (**B**) cell viability was determined using the Trypan blue exclusion assay. Results are presented as mean ± SD (n ≥ 4 independent experiments). (**C**) The escaped cells were photographed using a transmitted light microscope (Nikon DIAPHOT 300 equipped with a Nikon Digital sight-DS-Fi1 camera) (40X magnification). These invading cells were able to form new clusters (red arrows) and clusters could be linked together by isolated cells that emitted membrane extensions. The scale bar is 100μm. (**D**) Histograms represent the treatment-induced mitotic catastrophe (MC). Hematoxylin and eosin staining of invading cells allowed to detect morphologically abnormal nuclei (ie micro- and multinucleation) and the MC rate (in %) was determined for each therapeutic condition as the ratio of the number of mitotic catastrophe events to the total number of cells. Results are presented as mean ± SD (n ≥ 4 independent experiments). For graphs A, B and (**D**) # = significant difference between RT groups versus Ctrl group and * = significant difference between "with Au@DTDTPA(Gd) nanoparticles" groups versus 'w/o nanoparticles' groups at p < 0.05 according to the Mann–Whitney *U*-test. (**E**) Invading cells were fixed on T15 for immunocytochemistry experiments and analyzed by confocal microscopy: visualization of F-actin was performed using Alexa Fluor™ 488-conjugated Phalloidin (green), connexin 43 was detected using a primary anti-Cx43 antibody and an Alexa Fluor 555-conjugated secondary antibody (red) while nuclei were counterstained with Hoechst 33432. Irradiated cells (RT 2×5 Gy) showed actin-rich membrane protrusions and numerous punctate Cx43 signals at these extensions. When cells were exposed to Au@DTDTPA(Gd) nanoparticles, the organization of the actin cytoskeleton was strongly modified and Cx43 immunoreactivity corresponded to diffuse intracytoplasmic staining. White arrow heads show Cx43 signals. Images on the top line: the scale bar is 150μm; Inset: the scale bar is 75μm.

In parallel, immunocytochemistry experiments allow to characterize the membrane protrusions (Figure 3E): in RT groups, the thin and ultralong membrane protrusions were actin-rich tubular structures with punctate connexin 43 immunoreactivity along the protrusions. Considering the groups of spheroids receiving RT + NPs, Au@DTDTPA(Gd) nanoparticles seemed to interfere with the emission of cellular protrusions and connexin 43 immunoreactivity mainly corresponded to diffuse intracytoplasmic staining.

Aggressiveness and Recurrence Potential of Invading Tumor Cells Post-Irradiation Was Altered by Au@DTDTPA(Gd) Nanoparticles

To move through the brain parenchyma, invading glioma cells need remarkable plasticity and proteolytic activity. So, we analyzed the secretion and the activity of the matrix metalloproteinases MMP-2 and MMP-9 which reflect the proteolytic activity of escaped cells. Figure 4A represents gelatin zymography of conditioned media samples obtained from invading cells receiving different treatments. We detected the MMP2 proenzyme and active MMP2, as well as pro-MMP9 but to a lesser extent. For the densitometric quantification of the bands, we focused on MMP2 secretion (ie, we considered the sum of signals for MMP2 proenzyme and for active MMP2) (Figure 4B) and the active MMP2 (Figure 4C). Our results showed that MMP2 secretion and active MMP2 were lower in NPs-treated groups (without or with irradiation) than in other groups. These data suggest that Au@DTDTPA(Gd) nanoparticules can interfere with invasion by reducing proteolytic activity of invading cells that have escaped from U87 spheroids.

In parallel, we tried to determine whether any of the escaped cells might have stem-like features using the neurosphere assay, as previously described.[24] Briefly, U87 glioblastoma cells that had escaped from untreated or treated-spheroids (RT and/or AU@DTDTPA(Gd) nanoparticles) were resuspended in appropriate serum-free culture medium for 4 days. In these conditions, only glioma stem-like cells can enter into active proliferation and rapidly form floating neurospheres.[25] Considering untreated spheroids, we counted an average of 2230 neurospheres formed from $1{\times}10^5$ seeded invading cells (Figure 4D), suggesting that stem-like cells represented 2.2% of invading cells. Treatments markedly affected the ability of invading cells to form neurospheres. In particular, the number and the size of neurospheres were significantly reduced when spheroids were irradiated with 2×5 Gy or 10 Gy monodose regimen (ie, for $1{\times}10^5$ seeded invading cells, 1551 ± 236 neurospheres and 1151 ± 100 neurospheres were counted, respectively) (Figure 4D and E). Consistently with previous results, the exposure of U87 spheroids to Au@DTDTPA(Gd) nanoparticles further reduced the neurosphere forming ability which dropped to ~ 700 for « NPs + 2×5 Gy » and « NPs + 10 Gy » groups (ie, 665 ± 81 neurospheres; p = 0.029 for « NPs + 2×5 Gy » as compared to RT 2×5 Gy alone) (Figure 4D). Similarly, the average diameter of the neurospheres was smallest in these two treatment groups (Figure 4E). As the neurosphere assay is not sufficient to prove the presence of glioma stem cells,[26] preliminary experiments were performed to evaluate the influence of treatments on the Sox2 mRNA expression, as Sox2 is a transcription factor involved in the regulation of the maintenance of tumor stem cell properties.[27] The relative expression of Sox2 mRNA in escaped cells was decreased of about 25% when spheroids were treated by RT + NPs, as compared to RT alone (Table 2). Taken together, our results provide converging evidence that aggressiveness of glioblastoma cells is strongly reduced when U87 spheroids are exposed to Au@DTDTPA(Gd) nanoparticles before irradiation and show that the combined treatment is able to reduce the proportion of cells with stem-like features to less than 0.75%.

Discussion

Conventional X-ray radiotherapy is a keystone of glioblastoma treatment following the surgery resection. Unfortunately, at clinically tolerable doses, its efficacy remains insufficient to counteract the high radioresistance of these tumors. Radioresistance of GBM is often multifactorial and heterogeneous, including tumor cell-intrinsic factors as well as tumor microenvironment, and systematically leads to GBM recurrence. Recent researches have shown that brain tumors could form versatile multicellular tumor networks through two types of long intercellular membrane protrusions, ie, tumor microtubes and tunnelling nanotubes. Tumor microtubes are ultralong membrane protrusions (length >500 μm) wherein connexin 43 represents the most important gap junction protein.[28,29] They are used by glioma cells to drive tumour growth and invasion, resistance to standard therapies (including radiotherapy) and recurrence.[30] Elsewhere, several
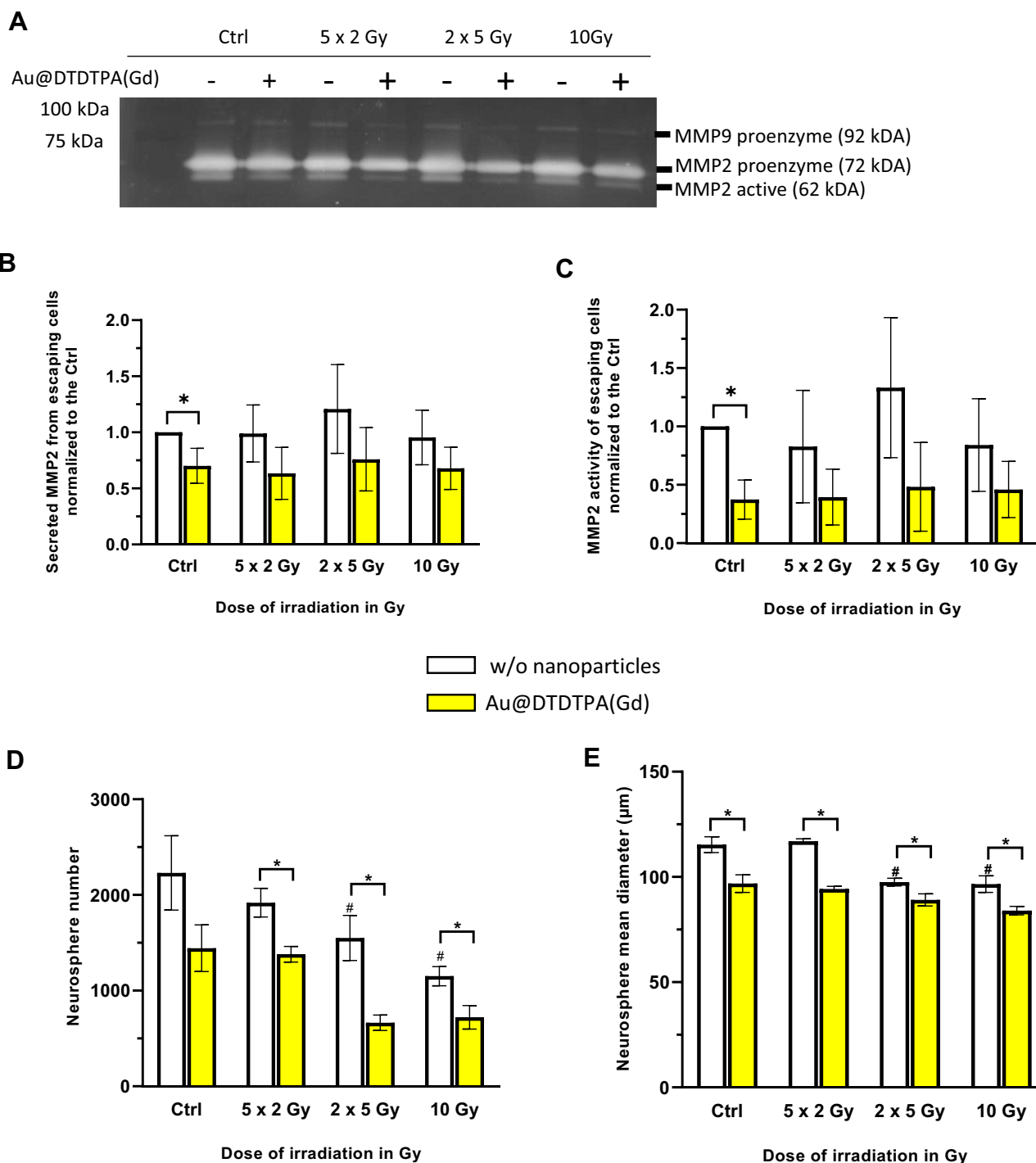
Figure 4 Impact of treatments on aggressiveness and recurrence potential of invading tumor cells. (**A-C**) Gelatin zymography method was carried out to assess gelatinases (MMP2 and MMP9) secretion and activity in invading cells supernatant. (**A**) 4 μg of total proteins obtained from supernatant of escaped cells were deposited in a 10% polyacrylamide gel with 1% porcine gelatin. Image of gel was acquired after migration for 2 hours and Coomassie Blue staining using a Doc XR+ Gel (Bio Rad, France). For each treatment condition, densitometric quantification of the bands allowed to determine (**B**) MMP2 secretion that corresponds to the sum of signals for MMP2 proenzyme and for active MMP2, and (**C**) active MMP2. Results are presented as mean ± SD (n = 4 independent experiments) (**D** and **E**) Assessment of the stem-like features of invading cells by neurosphere assay. After trypsinization, invading cells were recovered and counted. 1×10^5 invading cells were resuspended in appropriate serum-free culture medium for 4 days, allowing the formation of floating neurospheres. At the end of the experiment, (**D**) number and (**E**) size of neurospheres were measured using the GelCount® device (Oxford Optronix, UK). Results are presented as mean ± SD (n ≥ 4 independent experiments). For graphs B, C, D and (**E**) # = significant difference between RT groups versus Ctrl group and * = significant difference between "with Au@DTDTPA(Gd) nanoparticles" groups versus "w/o nanoparticles" groups at p < 0.05 according to the Mann–Whitney *U*-test.

Table 2 Effects of Treatments on Relative Expression of SOX2 mRNA

Therapeutic Groups	Mean ± SE
Control	1.00 ± 0.42
Au@DTDTPA(Gd) NPs	0.37 ± 0.08
RT 2×5 Gy	1.01± 0.97
RT 2×5 Gy + NPs	0.78 ± 0.32
RT 10 Gy	1.47 ± 0.63
RT 10 Gy + NPs	1.09 ± 0.31

experimental converging clues suggest that migration/invasion abilities of glioblastoma cells could be enhanced by conventional irradiation.[31–33] For example, Wank et al reported that 8 out of 10 glioblastoma cell lines (7 patient-derived primary GBM and 3 established cell lines) exhibited increased invasiveness after low-LET photon irradiation.[33] Despite the well-known limits of in vitro assays with established cell lines, our experiments seemed to be consistent with the emerging knowledges about resistance mechanisms in brain tumors. By applying several biological models (ie, 3D invasion assays, organotypic brain slice culture or chronic cranial window), our results showed that conventional X-ray radiotherapy, depending on dose fractionation, globally slowed down glioma progression: growth delays of the tumor/spheroid core were notable in vitro and in vivo as compared to control group and irradiation seemed to be able to reduce the number of escaping cells. Although less numerous, post-irradiation surviving cells remained very active: thus, the surface and distance of invasion were not decreased. Moreover, after radiotherapy, some of escaped cells were able to maintain intercellular connexion by emitting long actin-rich membrane protrusions, with morphological characteristics such as length >500 μm and expression connexin 43 protein that evoke tumor microtubes. In addition, about 1 to 1.5% of escaped cells post-irradiation gave rise to new tumor spheres. Taken together, our results show that surviving cells after irradiation were able to develop adaptative response allowing high invasiveness and aggressiveness.

Many preclinical and clinical investigations are ongoing to evaluate inorganic nanoparticles as radioenhancer agents in order to overcome radiotherapy resistance and limitations. In this context, we have evaluated the radiosensitizing potential of ultrasmall polyaminocarboxylate-coated gold nanoparticles, then labelled with Gd^{3+} ions named as Au@DTDTPA(Gd) nanoparticles when combined with conventional X-ray irradiation. In biological systems, radio-sensitizing effect of gold-based nanoparticles, quantitatively assessed from cell survival curves, is considered as the result of physical, chemical, and biological phenomena. Actually, several simulation studies have reported the enhanced emission of secondary electrons (such as Auger electrons, photo- or Compton electrons) following the radiation-induced ionization of gold nanoparticles and experimental works have shown catalytic surface processes (at least for AuNPs <5 nm in diameter) that boost water radiolysis and ROS formation:[34–36] secondary electrons and ROS have long been considered as responsible for increased DNA damage and compromised damage repair, and thus, for enhanced cell death. Recently, Pagacova et al have challenged this "mainstream" theory and demonstrated that the "classic DNA damage mechanism" was not sufficient to interpret the dose enhancement effect observed in vitro and in vivo, in particular the great increase in the life span of animals bearing intracerebral 9L gliosarcoma. They suggested that the radiosensitizing effect of ultrafine metal nanoparticles may rely on cytoplasmic processes, affecting subcellular organelles, rather than DNA damaging events.[37] In an original way, our study used various experimental approaches to provide new insights on the radiosensitizing effect of Au@DTDTPA(Gd) nanoparticles, focusing not only on the tumor bulk but also on the invading cells that spread into the surrounding brain parenchyma.

Our in vitro results, using 2D and 3D culture models, confirmed the radio-enhancement effect of these nanoparticles on U87 glioblastoma cells when combined to X-ray irradiation. Previously, Butterworth et al have established the radiosensitizing potential of Au@DTDTPA for 3 prostate cancers cell lines when cells were exposed to various doses of nanoparticles prior to irradiation with a single 4 Gy dose.[38] In addition, using the alkaline Comet assay, Miladi et al

showed that exposure to Au@DTDTPA or Au@DTDTPA(Gd) nanoparticles enhanced the amount of DNA damage in U87 cells submitted to ^{137}Cs-gamma radiation at two different doses (5 and 10 Gy).[15] In Miladi's work as well as in our study (data not shown), radio-enhancement effects obtained with Au@DTDTPA and Au@DTDTPA(Gd) nanoparticles were similar, suggesting that the radiosensitizing effect mainly stems from the interaction between X-photons and gold core whereas gadolinium ions contribute little or nothing to the radio-enhancement.

The model of U87-GFP spheroid under the chronic cranial window helped us to assess the radioresponse of brain tumors in vivo, including the infiltrative tumor area. In our conditions, the combination of Au@DTDTPA(Gd) and RT was not more efficient to reduce the main tumor mass than RT alone. The transient impact on tumor growth and the lack of proven local tumor control in vivo with the combined treatment (Au@DTDTPA(Gd) + RT 2×5 Gy) were disappointing. Actually, the benefit of the combined treatment RT+NPs was less remarkable in our work than that reported by Roux's research group with synchrotron-generated X-ray microbeams.[15,23] It could be explained (i) by insufficient intratumor accumulation of nanoparticles or (ii) by the higher radioresistance of the U87 cell line used. In addition, we assume that low dose rate of conventional X-rays irradiation was likely less favorable to physical interactions between ionizing radiation and gold nanoparticles, and led into less cellular damages than synchrotron-generated X-ray microbeams that allows for very high dose of irradiation at very high dose rate. Nonetheless, our model of chronic cranial window allowed to see differences in tumor boundaries between RT+NPs- and RT-treated groups. These observations let us suspect alterations in invasive behavior of glioblastoma cells and less diffuse infiltration after RT+NPs treatment. Further investigations confirmed that in case of RT + Au@DTDTPA(Gd), invasiveness was significantly reduced as compared to RT alone on different biological model. The present study corroborates in vitro studies reporting the reduction of cell migration of two carcinoma cell lines treated with gold nanoparticles in combination with 6 MV X-rays.[39,40] Further investigations revealed that Au@DTDTPA(Gd) nanoparticles were able to decrease the number and viability of tumor cells that escape and invade the surrounding brain parenchyma after irradiation. Precisely, combining Au@DTDTPA(Gd) nanoparticles with irradiation allows to significantly increase mitotic catastrophe. Mitotic catastrophe (MC) is defined as inopportune entry into mitosis despite the persistence of non-repaired DNA lesions, results in the loss of clonogenic ability and is considered as the main event that precedes radiation-induced cell death.[41–43] Our observations are consistent with previous published works reporting enhanced radiation-induced mitotic catastrophe after gold nanoparticles treatment.[44,45] Our data show that the long-term survival of invading cells is strongly impaired after RT+Au@DTDTPA(Gd) treatment, probably due to enhanced DNA-damages.

Recently, we have demonstrated on glioblastoma cells grown as monolayers that Au@DTDTPA(Gd) uptake induced a marked increase of the Young's modulus measured by atomic force microscopy and a decreased number of protrusions, causing an increased cell stiffness and impaired cell motility.[16] In the present study, when U87 spheroids were treated by RT+NPs, the living escaped cells appeared unable to form the interconnected network and we assume that similar mechanisms were involved. Moreover, living escaped cells exhibited reduced metalloprotease activity in RT+NPs groups. The decreased cell plasticity associated with the weak capacity of glioblastoma cells to degrade extracellular matrix likely explain the reduced invasiveness of these tumors when treated by RT+NPs. These findings are of major interest as they suggest that the combination of Au@DTDTPA(Gd) nanoparticles with irradiation could prevent the formation of tumor microtubes, which are strongly involved in radioresistance of glioblastomas. Multiphoton microscopy, a method of choice for minimally invasive monitoring of brain cell network activity over long periods of time in living animals,[46] is needed to confirm all these mechanisms in vivo after i.v. injection of Au@DTDTPA(Gd).

In glioblastoma, invading cells are considered as the major threat due to their high recurrence potential. Actually, Munthe et al have shown that migrating tumor cells in glioma biopsy material display a stem cell phenotype.[47] Combining Au@DTDTPA(Gd) nanoparticles with radiotherapy allowed to markedly reduce the ability of escaped cells to give rise new tumor spheres, and this was accompanied by a decrease in relative expression of Sox2 mRNA. These data suggest that combined treatment could affect the proportion of escaped cells with stem-like features. Even though further molecular investigations are required, these last results are particularly attractive in the context of glioblastoma therapy.

Conclusion

Beyond their role of « physical radiation dose enhancer», our results confirmed the attractive potential of Au@DTDTPA(Gd) nanoparticles as they could exert their radiosensitizing effect by altering the adaptive response

of glioma cells after irradiation. Indeed, exposure to Au@DTDTPA(Gd) nanoparticles prior to irradiation reduced the invasiveness and aggressiveness of glioblastoma cells, notably by (i) decreasing the number and viability of tumor cells that escape and can invade the surrounding brain parenchyma, (ii) preventing the ability of invading cells to form an interconnected network that is probably involved in GBM radioresistance (iii) altering their ability to give rise new tumor spheres. Although complementary experiments are needed to validate these mechanisms in vivo, Au@DTDTPA(Gd)-enhanced radiotherapy opens interesting perspectives for addressing the threat that invading cells pose in glioblastoma.

Data Sharing Statement

The raw/processed data required to reproduce these findings cannot be shared at this time due to technical or time limitations.

Acknowledgments

Author Contributions

All authors made a significant contribution to the work reported, whether that is in the conception, study design, execution, acquisition of data, analysis and interpretation, or in all these areas; took part in drafting, revising or critically reviewing the article; gave final approval of the version to be published; have agreed on the journal to which the article has been submitted; and agree to be accountable for all aspects of the work.

Disclosure

The authors declare no competing financial interests.

References

1. Cuddapah VA, Robel S, Watkins S, Sontheimer H. A neurocentric perspective on glioma invasion. *Nat Rev Neurosci*. 2014;15(7):455–465. doi:10.1038/nrn3765
2. Moncharmont C, Levy A, Guy JB, et al. Radiation-enhanced cell migration/invasion process: a review. *Crit Rev Oncol Hematol*. 2014;92(2):133–142. doi:10.1016/j.critrevonc.2014.05.006
3. Wank M, Schilling D, Schmid TE, et al. Human glioma migration and infiltration properties as a target for personalized radiation medicine. *Cancers*. 2018;10(11):456. doi:10.3390/cancers10110456
4. Minata M, Audia A, Shi J, et al. Phenotypic plasticity of invasive edge glioma stem-like cells in response to ionizing radiation. *Cell Rep*. 2019;26(7):1893–1905.e7. doi:10.1016/j.celrep.2019.01.076
5. Janjua TI, Rewatkar P, Ahmed-Cox A, et al. Frontiers in the treatment of glioblastoma: past, present and emerging. *Adv Drug Deliv Rev*. 2021;171:108–138. doi:10.1016/j.addr.2021.01.012
6. Ruiz-Garcia H, Ramirez-Loera C, Malouff TD, Seneviratne DS, Palmer JD, Trifiletti DM. Novel strategies for nanoparticle-based radiosensitization in glioblastoma. *Int J Mol Sci*. 2021;22(18):9673. doi:10.3390/ijms22189673
7. University Hospital, Grenoble. Radiotherapy of multiple brain metastases using AGuIX® gadolinium-chelated polysiloxane based nanoparticles: a prospective randomized Phase II clinical trial; 2021. https://clinicaltrials.gov/ct2/show/NCT03818386. Accessed January 25, 2022.
8. Zhang P, Marill J, Darmon A, Mohamed Anesary N, Lu B, Paris S. NBTXR3 radiotherapy-activated functionalized Hafnium Oxide nanoparticles show efficient antitumor effects across a large panel of human cancer models. *Int J Nanomedicine*. 2021;16:2761–2773. doi:10.2147/IJN.S301182
9. Liu Y, Zhang P, Li F, et al. Metal-based nanoenhancers for future radiotherapy: radiosensitizing and synergistic effects on tumor cells. *Theranostics*. 2018;8(7):1824–1849. doi:10.7150/thno.22172
10. Schuemann J, Berbeco R, Chithrani DB, et al. Roadmap to clinical use of gold nanoparticles for radiation sensitization. *Int J Radiat Oncol Biol Phys*. 2016;94(1):189–205. doi:10.1016/j.ijrobp.2015.09.032
11. Lux F, Tran VL, Thomas E, et al. AGuIX® from bench to bedside-Transfer of an ultrasmall theranostic gadolinium-based nanoparticle to clinical medicine. *Br J Radiol*. 2019;92(1093):20180365. doi:10.1259/bjr.20180365
12. Penninckx S, Heuskin AC, Michiels C, Lucas S. Gold nanoparticles as a potent radiosensitizer: a transdisciplinary approach from physics to patient. *Cancers*. 2020;12(8):2021. doi:10.3390/cancers12082021
13. Rosa S, Connolly C, Schettino G, Butterworth KT, Prise KM. Biological mechanisms of gold nanoparticle radiosensitization. *Cancer Nano*. 2017;8(1):2. doi:10.1186/s12645-017-0026-0
14. Alric C, Taleb J, Le Duc G, et al. Gadolinium Chelate Coated Gold Nanoparticles As Contrast Agents for Both X-ray Computed Tomography and Magnetic Resonance Imaging. *J Am Chem Soc*. 2008;130(18):5908–5915. doi:10.1021/ja078176p
15. Miladi I, Alric C, Dufort S, et al. The In Vivo Radiosensitizing Effect of Gold Nanoparticles Based MRI Contrast Agents. *Small*. 2014;10(6):1116–1124. doi:10.1002/smll.201302303

16. Durand M, Lelievre E, Chateau A, et al. The detrimental invasiveness of glioma cells controlled by gadolinium chelate-coated gold nanoparticles. *Nanoscale*. 2021;13(20):9236–9251. doi:10.1039/D0NR08936B

17. Retif P, Pinel S, Toussaint M, et al. Nanoparticles for radiation therapy enhancement: the key parameters. *Theranostics*. 2015;5(9):1030–1044. doi:10.7150/thno.11642

18. Eisemann T, Costa B, Strelau J, Mittelbronn M, Angel P, Peterziel H. An advanced glioma cell invasion assay based on organotypic brain slice cultures. *BMC Cancer*. 2018;18:103. doi:10.1186/s12885-018-4007-4

19. Livak KJ, Schmittgen TD. Analysis of relative gene expression data using real-time quantitative PCR and the 2(-Delta Delta C(T)) Method. *Methods*. 2001;25(4):402–408. doi:10.1006/meth.2001.1262

20. Li Y, Baran U, Wang RK. Application of Thinned-Skull Cranial Window to Mouse Cerebral Blood Flow Imaging Using Optical Microangiography. *PLoS One*. 2014;9(11):e113658. doi:10.1371/journal.pone.0113658

21. Holtmaat A, Bonhoeffer T, Chow DK, et al. Long-term, high-resolution imaging in the mouse neocortex through a chronic cranial window. *Nat Protoc*. 2009;4(8):1128–1144. doi:10.1038/nprot.2009.89

22. Mostany R, Portera-Cailliau C. A method for 2-photon imaging of blood flow in the neocortex through a cranial window. *J Vis Exp*. 2008;1(12):678. doi:10.3791/678

23. Jiménez Sánchez G, Maury P, Stefancikova L, et al. Fluorescent radiosensitizing gold nanoparticles. *Int J Mol Sci*. 2019;20(18):E4618. doi:10.3390/ijms20184618

24. Galli R. The Neurosphere Assay (NSA) Applied to Neural Stem Cells (NSCs) and Cancer Stem Cells (CSCs). *Methods Mol Biol*. 2019;1953:139–149. doi:10.1007/978-1-4939-9145-7_9

25. Soares R, Ribeiro FF, Lourenço DM, et al. The neurosphere assay: an effective in vitro technique to study neural stem cells. *Neural Regen Res*. 2021;16(11):2229–2231. doi:10.4103/1673-5374.310678

26. Ishiguro T, Ohata H, Sato A, Yamawaki K, Enomoto T, Okamoto K. Tumor-derived spheroids: relevance to cancer stem cells and clinical applications. *Cancer Sci*. 2017;108(3):283–289. doi:10.1111/cas.13155

27. Lopez-Bertoni H, Johnson A, Rui Y, et al. Sox2 induces glioblastoma cell stemness and tumor propagation by repressing TET2 and deregulating 5hmC and 5mC DNA modifications. *Sig Transduct Target Ther*. 2022;7(1):1–12. doi:10.1038/s41392-021-00857-0

28. Osswald M, Jung E, Sahm F, et al. Brain tumour cells interconnect to a functional and resistant network. *Nature*. 2015;528(7580):93–98. doi:10.1038/nature16071

29. Weil S, Osswald M, Solecki G, et al. Tumor microtubes convey resistance to surgical lesions and chemotherapy in gliomas. *Neuro-Oncology*. 2017;19(10):1316–1326. doi:10.1093/neuonc/nox070

30. Venkataramani V, Schneider M, Giordano FA, et al. Disconnecting multicellular networks in brain tumours. *Nat Rev Cancer*. 2022;22(8):481–491. doi:10.1038/s41568-022-00475-0

31. Goetze K, Scholz M, Taucher-Scholz G, Mueller-Klieser W. The impact of conventional and heavy ion irradiation on tumor cell migration in vitro. *Int J Radiat Biol*. 2007;83(11–12):889–896. doi:10.1080/09553000701753826

32. De Bacco F, Luraghi P, Medico E, et al. Induction of MET by ionizing radiation and its role in radioresistance and invasive growth of cancer. *J Natl Cancer Inst*. 2011;103(8):645–661. doi:10.1093/jnci/djr093

33. Wank M, Schilling D, Reindl J, et al. Evaluation of radiation-related invasion in primary patient-derived glioma cells and validation with established cell lines: impact of different radiation qualities with differing LET. *J Neurooncol*. 2018;139(3):583–590. doi:10.1007/s11060-018-2923-4

34. Misawa M, Takahashi J. Generation of reactive oxygen species induced by gold nanoparticles under x-ray and UV Irradiations. *Nanomedicine*. 2011;7(5):604–614. doi:10.1016/j.nano.2011.01.014

35. Gilles M, Brun E, Sicard-Roselli C. Quantification of hydroxyl radicals and solvated electrons produced by irradiated gold nanoparticles suggests a crucial role of interfacial water. *J Colloid Interface Sci*. 2018;525:31–38. doi:10.1016/j.jcis.2018.04.017

36. Gerken LRH, Gogos A, Starsich FHL, et al. Catalytic activity imperative for nanoparticle dose enhancement in photon and proton therapy. *Nat Commun*. 2022;13(1):3248. doi:10.1038/s41467-022-30982-5

37. Pagáčová E, Štefančíková L, Schmidt-Kaler F, et al. Challenges and contradictions of metal nano-particle applications for radio-sensitivity enhancement in cancer therapy. *Int J Mol Sci*. 2019;20(3):588. doi:10.3390/ijms20030588

38. Butterworth KT, Nicol JR, Ghita M, et al. Preclinical evaluation of gold-DTDTPA nanoparticles as theranostic agents in prostate cancer radiotherapy. *Nanomedicine*. 2016;11(16):2035–2047. doi:10.2217/nnm-2016-0062

39. Shahhoseini E, Feltis BN, Nakayama M, et al. Combined effects of gold nanoparticles and ionizing radiation on human prostate and lung cancer cell migration. *Int J Mol Sci*. 2019;20(18):4488. doi:10.3390/ijms20184488

40. Shahhoseini E, Nakayama M, Piva TJ, Geso M. Differential effects of gold nanoparticles and ionizing radiation on cell motility between primary human colonic and melanocytic cells and their cancerous counterparts. *Int J Mol Sci*. 2021;22(3):1418. doi:10.3390/ijms22031418

41. Ianzini F, Mackey MA. Spontaneous premature chromosome condensation and mitotic catastrophe following irradiation of HeLa S3 cells. *Int J Radiat Biol*. 1997;72(4):409–421. doi:10.1080/095530097143185

42. Ianzini F, Mackey MA. Delayed DNA damage associated with mitotic catastrophe following X-irradiation of HeLa S3 cells. *Mutagenesis*. 1998;13(4):337–344. doi:10.1093/mutage/13.4.337

43. Castedo M, Perfettini JL, Roumier T, Andreau K, Medema R, Kroemer G. Cell death by mitotic catastrophe: a molecular definition. *Oncogene*. 2004;23(16):2825–2837. doi:10.1038/sj.onc.1207528

44. Paquot H, Daouk J, Chateau A, Retif P, Barberi-Heyob M, Pinel S. Radiation-induced mitotic catastrophe enhanced by gold nanoparticles: assessment with a specific automated image processing workflow. *Radiat Res*. 2019;192(1):13–22. doi:10.1667/RR14962.1

45. Kunoh T, Shimura T, Kasai T, et al. Use of DNA-generated gold nanoparticles to radiosensitize and eradicate radioresistant glioma stem cells. *Nanotechnology*. 2019;30(5):055101. doi:10.1088/1361-6528/aaedd5

46. Larson AM. Multiphoton microscopy. *Nature Photon*. 2011;5(1):1. doi:10.1038/nphoton.an.2010.2

47. Munthe S, Sørensen MD, Thomassen M, et al. Migrating glioma cells express stem cell markers and give rise to new tumors upon xenografting. *J Neurooncol*. 2016;130(1):53–62. doi:10.1007/s11060-016-2221-y